

Three-Dimensional Simulation of Earthquakes on the Los Angeles Fault System

by Kim B. Olsen and Ralph J. Archuleta

Abstract We have used a 3D finite-difference method to simulate ground motion from elastodynamic propagating ruptures with constant slip on faults in the metropolitan area of Los Angeles, California. Simulations are carried out for hypothetical M 6.75 earthquakes on the Palos Verdes and Elysian Park faults and, for comparison, an approximation to the 17 January 1994 M 6.7 Northridge earthquake. The dominant subsurface features of this area are the deep sedimentary Los Angeles basin and the smaller and shallower San Fernando basin. Simulated ground motions are restricted to the frequency range 0.0 to 0.4 Hz.

Ground-motion time histories show that, in general, sites associated with the largest particle velocities and cumulative kinetic energies are located (1) in the epicentral area, (2) above the deepest parts of the basins, and (3) near the steepest edges of the Los Angeles basin. We find maximum particle velocities for the Palos Verdes, Elysian Park, and Northridge simulations of 0.44, 0.67, and 0.58 m/sec, respectively. In each case, both the directivity of the rupture and the lower impedance of the basins significantly amplify the ground motion. Although the gross radiation pattern from these ruptures is observable, the 3D basin structure distorts the wave field and becomes a source for edge-generated waves. Signal durations at some basin sites last beyond 90 sec due to Love waves and refracted S waves that propagate into the sediments from the basin edges. Compared with the Palos Verdes event, the durations are generally smaller for the Elysian Park earthquake due to a smaller amount of Love waves generated at the basin edges.

A simple approximation to the Northridge earthquake reproduces the overall spatial pattern of the long-period particle velocities, successfully predicts the timing of late-arriving waves, and matches the peak velocities with discrepancies generally less than a factor of 2. However, for localized areas immediately north and south of the Santa Monica Mountains, the computed ground motion underpredicts the observed horizontal peak velocities but matches the vertical ones. The pattern of simulated total cumulative kinetic energies is similar to that for the damage intensities observed near the epicenter of the Northridge event. While the Northridge earthquake caused damage in the Los Angeles area, the 3D simulations show that earthquakes with the same magnitude on the Palos Verdes or Elysian Park faults produce more severe ground shaking in the Los Angeles basin.

Introduction

The metropolitan area of the greater Los Angeles area is characterized by a complex geology and the proximity of numerous active faults (hereafter referred to as the Los Angeles fault system). Until recently, the hazards due to rupture on these faults have been considered somewhat less important than those caused by a rupture of the San Andreas fault (Working Group on California Earthquake Probabilities (WGCEP), 1995). However, earthquakes on faults within the Los Angeles region, such as the 1971 San Fernando (M 6.7),

the 1987 Whittier Narrows (M 5.9), and the 1994 (M 6.7) Northridge earthquake, have changed this picture (WGCEP, 1995). For example, Dolan *et al.* (1995) estimate that the Los Angeles fault system has a collective average recurrence interval for M 7.2 to 7.5 earthquakes similar to that of an M 7.2 to 7.5 earthquake on the San Andreas fault, although none of the faults cited by Dolan *et al.* (1995) have produced a major earthquake in historical time. Because of the proximity of the faults within the greater Los Angeles area, it is

likely that the damage in the Los Angeles metropolitan area from rupture on one or more of these faults will be more severe than that caused by a larger-magnitude earthquake on the San Andreas fault (e.g., Dolan *et al.*, 1995; Heaton *et al.*, 1995). Thus, it is important to predict the ground motion resulting from hypothetical earthquakes on the Los Angeles fault system.

One of the most difficult problems with predicting ground motion in the Los Angeles area is the three-dimensional nature of the velocity structure, especially the deep sedimentary basins (Yerkes *et al.*, 1965; Wright, 1991). The interaction between basins and wave propagation has been the subject of numerous articles (see Sánchez-Sesma and Luzón, 1995, and references therein). Until recently, almost all ground-motion studies that simulated earthquakes as propagating ruptures on a finite fault have been limited to a one-dimensional velocity model that did not account the more realistic basin structure (e.g., Archuleta and Day, 1980; Olson and Apsel, 1982; Hartzell and Heaton, 1983, 1986; Archuleta, 1984; Hartzell and Iida, 1990; Beroza, 1991; Steidl *et al.*, 1991; Wald *et al.*, 1991; Takeo and Kanamori, 1995; Wald *et al.*, 1996; Heaton *et al.*, 1995). When more complicated 2D or 3D velocity structures are used, the earthquake source is generally limited to excitation by a plane wave or a point source.

Studies of ground motion in sedimentary basins have generally used point or planar sources. Vidale and Helmberger (1988) approximated the 1971 San Fernando earthquake as a point source and propagated waves (0.1 to 0.5 Hz) across a 2D cross section of the San Fernando Valley and Los Angeles basins using a finite-difference method. The same approach has been applied to other earthquakes: Schrivner and Helmberger (1994) simulated ground motion in the Los Angeles basin from the 4 October 1987 Whittier Narrows aftershock (M 5.3) and the 28 June 1991 Sierra Madre mainshock (M 5.8); Pitarka *et al.* (1994) simulated ground motion in the Ashigara Valley from the 5 August 1990 Odawara, Japan, earthquake. The 2D finite-difference method was extended to 3D by Olsen and Schuster (1992, with extended references), who simulated wave propagation in the Salt Lake Basin for mine blasts and plane waves. Frankel and Vidale (1992) simulated 3D wave propagation in the Santa Clara Valley using a far-field point source. Yomogida and Etgen (1993) applied this method to the Los Angeles Basin in simulating the 1987 Whittier-Narrows earthquake. Frankel (1993) took the next step when he simulated 3D elastic waves in the San Bernardino basin from a hypothetical M 6.5 earthquake on the San Andreas fault. Although the source model was nearly a line source (30-km long and 3-km wide) and the model depth was limited to 7 km, Frankel included both a 3D velocity structure and a propagating rupture over a finite fault area. The first integration of the full 3D regional velocity structure of the Los Angeles area with earthquake rupture on a finite fault was carried out by Olsen *et al.* (1995b). Using a parallel supercomputer, they simulated 0 to 0.4-Hz ground motion for an M 7.75 earth-

quake along a 170-km-long stretch of the San Andreas fault from Tejon Pass to San Bernardino. While all of the 3D studies have been limited to low frequencies ($f \leq 1.0$ Hz) or very limited spatial volume, due to extensive computational requirements, these studies demonstrated significant 3D effects from the basin structures. These effects include a strong correlation between the duration of shaking and the site location within the basin and the generation of surface waves at the basin edges. Thus, given the severe 3D subsurface structure and large earthquakes on extended faults in the Los Angeles area, realistic estimates of the ground motion from future earthquakes require 3D modeling.

In this study, we simulate ground motion for three hypothetical M 6.75 earthquakes on the Los Angeles fault system. We consider the following kinematic ruptures: strike-slip on the Palos Verdes fault, blind thrust on the Elysian Park fault, and blind thrust on the Oak Ridge fault (Northridge). The first two hypothetical earthquakes have recently been used as scenario events for ground-motion calculations by the Southern California Earthquake Center (SCEC) and are "geologically reasonable scenarios" defined by Dolan *et al.* (1995). The third simulation is a simple approximation to the Northridge earthquake. We use a complex 3D geological model of the Los Angeles area developed by Magistrale *et al.* (1996). The kinematic earthquake rupture and elastic wave propagation are numerically modeled using a 3D finite-difference method (Olsen, 1994).

Los Angeles Area Elastic Model

We use a 3D elastic model of the Los Angeles area assembled by Magistrale *et al.* (1996). The spatial resolution of the model is approximately 0.5 km (H. Magistrale, written comm., 1995). The model parameters outside and below the sedimentary basins are assigned according to the 1D regional model of Hadley and Kanamori (1977). Within the basins, the P -wave velocity is determined from the depths and ages estimated for four geological horizons (Faust, 1951) and calibrated with local P -wave velocity models for the basins. The density is estimated from the P -wave velocity using the Nafe-Drake relation (Nafe and Drake, 1960). Finally, the S -wave velocity is computed from the P -wave velocity and the Poisson's ratio (Ludwig *et al.*, 1970). Although we realize that the surficial sediments have lower velocities, numerical considerations impose a minimum S -wave velocity of 1.0 km/sec at the Earth's surface; the corresponding P -wave velocity is 2.4 km/sec.

Figure 1a shows a topographic map of southern California. The rectangular area outlined by the dashed line is the region being modeled. The reference frame of the model (note Figs. 1a and 1b) is rotated 28° counterclockwise from the north to minimize the computational requirements for the simulations. Azimuths of 118° and 28° are within 10° of the strike-parallel and strike-perpendicular components, respectively, for the three faults considered in this study. The axis of the main basin trough trends approximately 118° as

does the San Andreas fault, which is just beyond the northeast boundary of the area being modeled. Throughout this article, we use azimuths of 118° and 28° to analyze the horizontal ground motion for the three earthquake simulations.

The 3D nature of the model is characterized in Figure 1c by an isotach surface corresponding to an S-wave velocity of 2.6 km/sec. The large depression is the Los Angeles basin; the smaller basin to the northwest is the San Fernando basin separated from the Los Angeles basin by the Santa Monica Mountains. In these simulations, the topography above sea level is not included.

Modeling Parameters

The physical model is discretized with a grid spacing of 0.4 km, equivalent to 6.5 nodes per minimum shear wavelength of 2.5 km, which limits the numerical dispersion error to less than about 12% (Olsen, 1994) and results in a maximum resolved frequency of 0.4 Hz. The full model, approximately $155 \times 134 \times 34$ km, is discretized into $388 \times 337 \times 85$ ($= 11,114,260$ million) grid points. Absorbing boundary conditions (Clayton and Engquist, 1977) are applied to the sides of the computational model. To further reduce artificial reflections, the boundaries of the model are padded with a 40 to 50-point-wide zone of attenuative material (Cerjan *et al.*, 1985). We restrict our interpretations to the area 95×115 km (area shown within the rectangle, Fig. 1a) to exclude boundary effects. Except for the boundary regions, where the waves are artificially damped, there is no attenuation in the Earth model. The 3D modeling parameters are listed in Table 1.

We use a staggered-grid finite-difference scheme to solve the 3D elastic equations of motion (Levander, 1988); the accuracy is fourth-order in space and second-order in time. The velocity-stress finite-difference staggered-grid method (second-order in space) for a homogeneous material was first described by Madariaga (1976) with its natural extension to inhomogeneous media given by Virieux (1984, 1986) and to fourth-order accuracy given by Levander (1988). The exact numerical implementation of the 3D scheme is described in Olsen (1994). Simulations were carried out on an SGI Powerchallenge supercomputer using approximately 500 Mbytes of physical memory.

The source is implemented in the finite-difference grid by adding

$$-M_{ij}(t)/V$$

to $S_{ij}(t)$, where $M_{ij}(t)$ is the ij th component of the moment tensor for the earthquake, $V = dx^3$ is the cell volume, and $S_{ij}(t)$ is the ij th component of the stress tensor on the fault at time t . We use a Gaussian-shaped slip rate in the 3D simulations with a bandwidth of 0.0 to 0.4 Hz (Fig. 2). The slip-rate function is constant everywhere on the fault. This allows the seismic moment and all of the synthetics to be scaled by a single value of slip. The effective rise time is about 3 sec

everywhere on the fault. The slip rate (likewise the slip) tapers to zero over a distance of 400 m at the edges of the fault. The rupture is radially propagated out from the hypocenter (i_h, j_h, k_h) at time $t = 0$ to the remaining grid points on the fault (i_f, j_f, k_f) at a rate of

$$V_r(i_f, j_f, k_f) = 0.85V_s(i_f, j_f, k_f),$$

where $V_s(i_f, j_f, k_f)$ is the shear-wave velocity at (i_f, j_f, k_f) .

To allow for comparisons with sources with a different slip-rate function, we deconvolved the Gaussian source time function from the synthetic records. The deconvolved source spectrum is shown by the dashed line in Figure 2. The source has a constant spectral response to displacement for frequencies between 0.0 and 0.4 Hz.

Three Earthquake Scenarios

In this section, we examine the particle velocity wave fields from three hypothetical earthquakes within the Los Angeles fault system (Fig. 1b). Each earthquake—strike-slip on the Palos Verdes fault, blind thrust on the Elysian Park fault, and blind thrust on the Oak Ridge fault (Northridge)—has the same moment magnitude (Northridge is M 6.7; Palos Verdes and Elysian Park are M 6.75). The difference in the computed ground-motion results from the style of faulting, the extent of the rupture, and the location of the fault within the Los Angeles region. We examine all three components of particle velocity ground motion: vertical (up being positive), 118° horizontal, and 28° horizontal. The ground motion is computed for 90 sec starting at the origin time of the earthquake. Map view snapshots of the wave field are shown for all three components. In addition to the snapshots, velocity seismograms are shown along two profiles A-B and C-D (Fig. 1b) for the hypothetical ruptures on the Palos Verdes and Elysian Park faults. The synthetics from the Northridge event simulation are compared directly with data that have been lowpass-filtered to the same frequency range. The fault and rupture parameters for each earthquake scenario are given in Table 2.

While simulating the effects of the Northridge earthquake is a natural application for our modeling, we have selected the other two earthquake scenarios as part of the Southern California Earthquake Center (SCEC) objective of computing time histories for possible damaging earthquakes in the Los Angeles region. It is not obvious, *a priori*, which earthquake presents a greater hazard even though both have identical seismic moments. The Palos Verdes earthquake and the Elysian Park earthquake represent different styles of faulting and geometries. Thus, one would expect the basins to affect the ground motion in very different ways. This article examines such differences.

Palos Verdes Earthquake

The Palos Verdes fault is a major strike-slip fault on the southwestern edge of the Los Angeles metropolitan area.

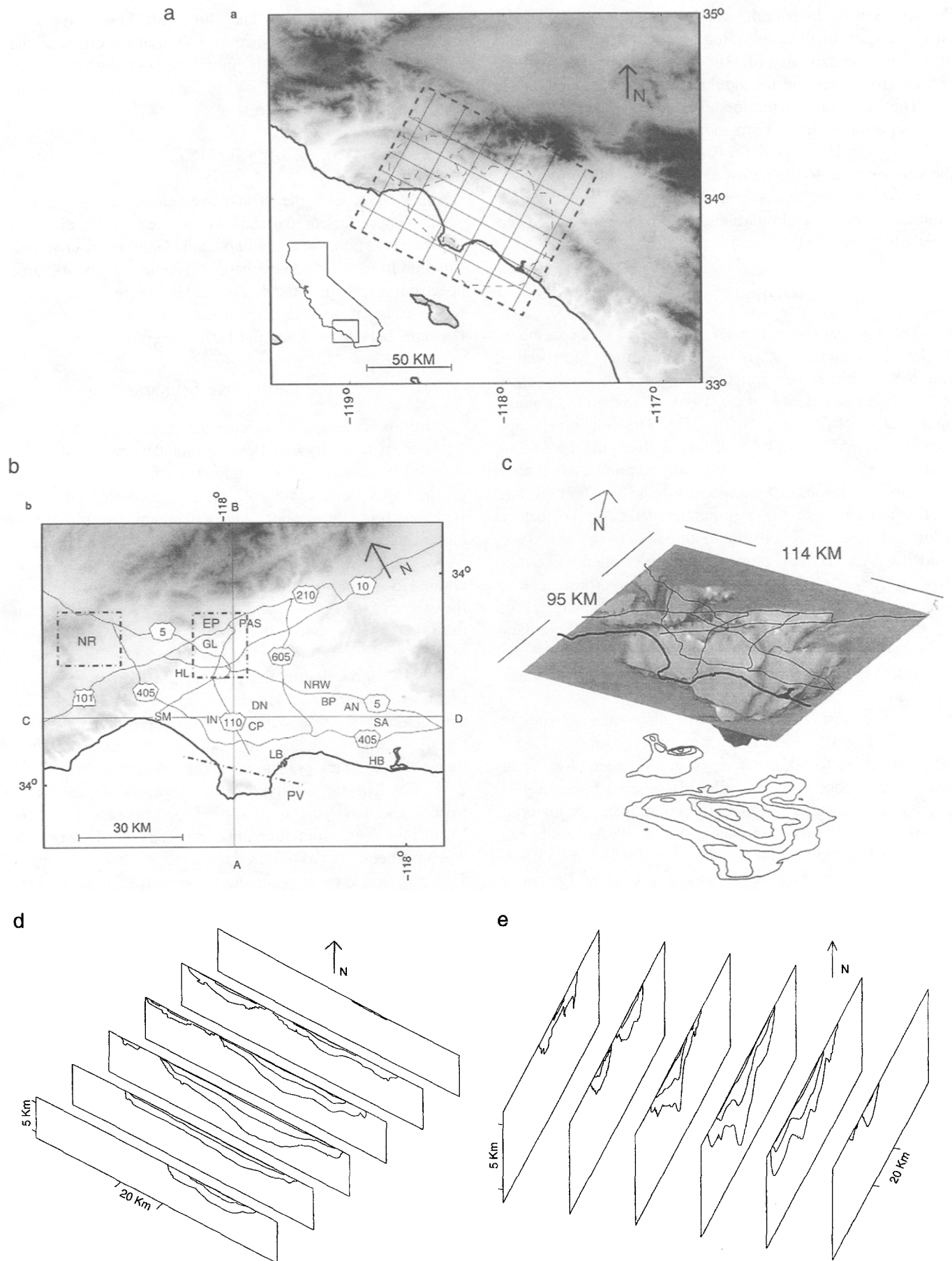


Figure 1. Los Angeles area model. (a) Topographic map of southern California centered on the Los Angeles region. The dashed rectangle shows the areal extent of the basin model used in this study. The thin dashed contour shows the outline of the basin region, represented by the trace of the isosurface for an *S*-wave velocity of 2.6 km/sec. The thin solid lines depict the profiles used to display vertical cross sections of the model in (d) and (e). (b) Topographic map of the Los Angeles area model. The dash-dot lines show the surface projections of the three faults where we have simulated ruptures in this study: the Palos Verdes fault (PV), the Elysian Park fault (EP), and the Oak Ridge fault that ruptured during the 17 January 1994 Northridge event (NR). The thin solid lines depict major freeways in the modeling area. Lines A-B and C-D are profiles used for displaying seismograms. AN is Anaheim, BP is Buena Park, CP is Compton, DN is Downey, GL is Glendale, HB is Huntington Beach, HL is Hollywood, IN is Inglewood, LB is Long Beach, NRW is Norwalk, PAS is Pasadena, SA is Santa Ana, and SM is Santa Monica. (c) 3D perspective and contour map (contour interval 1 km, shallowest contour at a depth of 1 km) of the isosurface for an *S*-wave velocity of 2.6 km/sec. The thin lines on the map show major freeways in the Los Angeles area, and the thick line is the coastline. (d) and (e) Vertical cross sections along 118° and 28°, respectively, with contours of *S*-wave velocities of 1.0, 2.0, and 3.0 km/sec. The 3D modeling parameters are listed in Table 1.

Table 1
3D Modeling Parameters

Spatial discretization (km)	0.4
Temporal discretization (sec)	0.025
Lowest <i>P</i> -wave velocity (km/sec)	2.41
Lowest <i>S</i> -wave velocity (km/sec)	1.00
Lowest density (kg/m ³)	2070
Number of grid points along 118°	388
Number of grid points along 28°	337
Number of grid points along vertical	85
Number of time steps	3600
Simulation time (sec)	90

Recent studies indicate a slip rate of 3 mm/yr on the Palos Verdes fault (Stephenson *et al.*, 1995). This slip rate can be compared with 1.2 mm/yr or less on the Newport-Inglewood fault (Dolan *et al.*, 1995), which has been considered one of the major hazards for the Los Angeles metropolitan area (Ziony, 1985). Because of its rather high slip rate, the Palos Verdes fault is a prime candidate for producing a damaging earthquake.

We simulate the Palos Verdes earthquake as a bilateral, pure strike-slip rupture on a vertical fault plane that is 35-km long. The Palos Verdes fault is not perfectly aligned with the 118° coordinate. Thus, motion that is referred to as strike parallel or fault perpendicular is only approximate. The fault plane extends from a depth of 0.5 to 16.5 km. The rupture

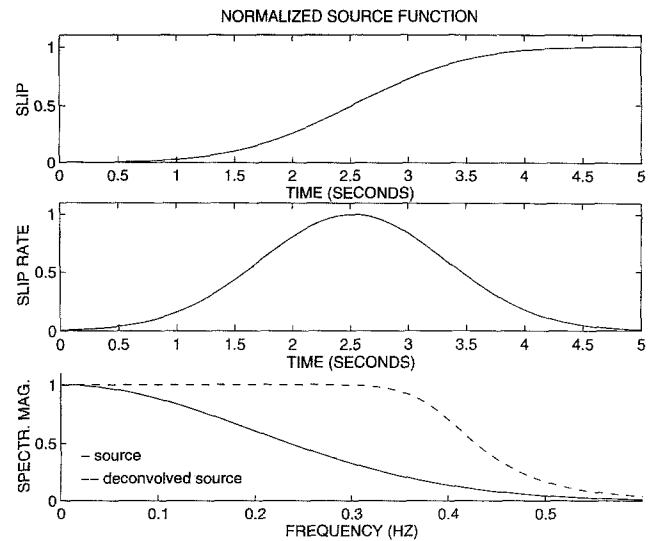


Figure 2. The normalized slip (top) and slip-rate functions (middle), and the velocity spectrum (bottom) of the Gaussian wavelet used in the 3D simulations. The dashed line shows the source spectrum after deconvolution of the Gaussian wavelet and low-pass-filtering with a corner frequency of 0.4 Hz.

Table 2
Earthquake Rupture Parameters

	Simulation		
	Palos Verdes	Elysian Park	Northridge
Hypocenter longitude (°)	-118.332	-118.203	-118.544
Hypocenter latitude (°)	33.785	34.105	34.210
Hypocenter depth (km)	7.2	15.0	18.5
Moment magnitude	6.75	6.75	6.7
Width (km)	16	21	22
Length (km)	35	16	18
Depth to top of fault (km)	0.5	10.5	6.0
Dip (°)	90	25	40
Strike (°)	141	298	118
Rake (°)	180	90	101

initiates at a depth of 7.2 km midway between the ends of the fault. The rupture reaches the ends of the fault in about 10 sec, and the static offset is established everywhere on the fault by about 13 sec after the origin time. As will be seen in later figures, the directivity effect is quite pronounced on the 28° horizontal. However, because the rupture initiates at depth and propagates toward the free surface, there is a directivity effect on the 118° component. This directivity coupled with the lower shear modulus of the surficial sediments significantly amplifies the ground velocity.

Snapshots of the three components of motion are shown in Figure 3. The classical double-couple radiation pattern for a right-lateral strike-slip fault is evident in the snapshots at 7 and 10 sec. The strike-parallel motion (approximately 118°) is discontinuous across the fault with positive motion to the southeast; the fault-perpendicular motion (approximately 28°) is continuous across the fault but has opposite

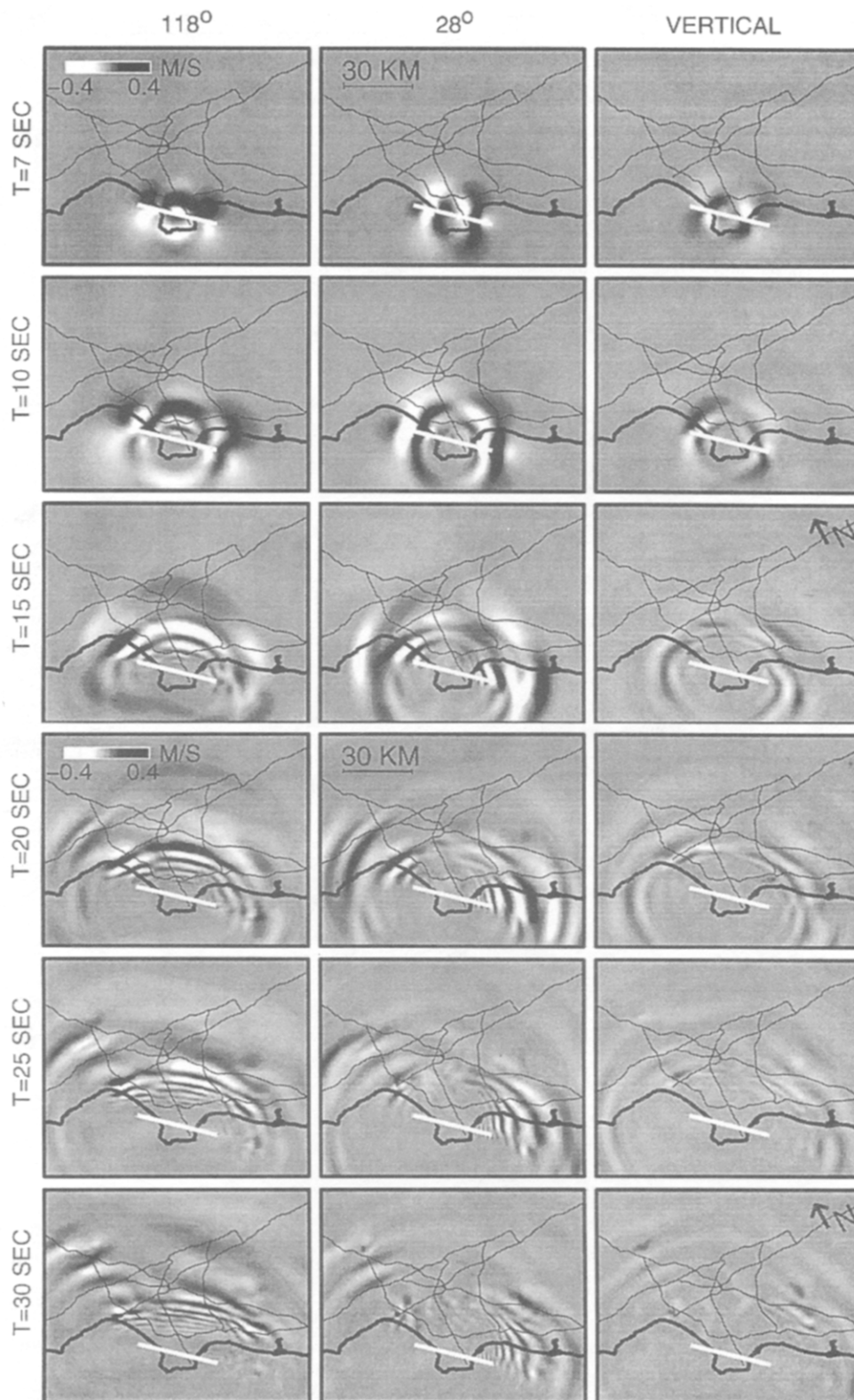


Figure 3. Snapshots of simulated wave propagation in the Los Angeles area for a constant-slip rupture on the Palos Verdes fault; the snapshots depict velocities along 118° and 28° and vertical from 7.5 to 90 sec after the origin time of the rupture. Light (dark) shading depicts negative (positive) particle velocity. The particle motion is scaled by a constant for all snapshots. The thick white line depicts the surface trace of the fault. The thin lines on the map show major freeways in the Los Angeles area. *L* depicts basin-edge-induced waves; *R* denotes localized areas of resonance.

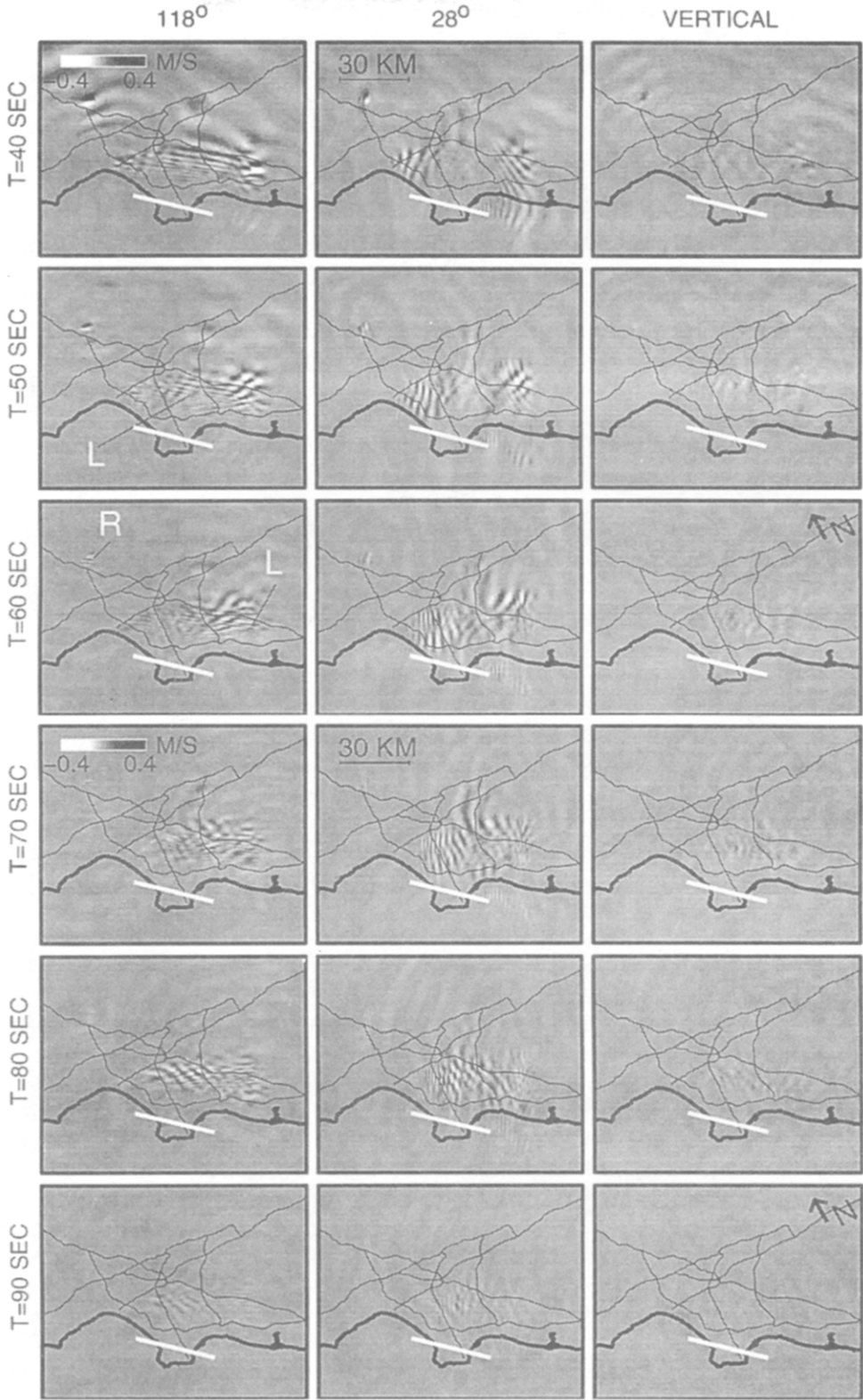


Figure 3. Continued

polarity from one end of the fault to the other; the vertical motion shows the four-lobed pattern in the faint *P*-wave field with more intense motion, with opposite polarity, resulting from the more slowly propagating *SV* motion. The *S*-wave amplitudes dominate each of the frames; the vertical component is much smaller, as expected from a purely strike-slip rupture mechanism. By 20 sec, the edges of the basins are beginning to distort the circular wave fronts of the *S* wave. Thereafter, the seismic waves generate a much more complex pattern in the main trough of the basin. The 3D structure of the Los Angeles basin establishes and sustains two primary patterns. The fault-parallel (118°) motion is concentrated along the axis of the basin. In cultural terms, the motion is concentrated just southwest and parallel to the I-5 freeway in the region near the cities of Downey, Norwalk, Buena Park, Anaheim, and Santa Ana. The fault-perpendicular motion (28°) has a northeast-southwest orientation and is localized in two disparate regions—just near Santa Monica and Inglewood and in northern Orange County near the cities of Anaheim, Santa Ana, and Huntington Beach.

It is instructive to relate the 3D structure and the ground motion by examining the seismic record sections along profiles A-B and C-D, Figures 4a and 4b, respectively. Profile A-B (Fig. 1b) extends 95 km from south of the Palos Verdes fault, almost bisecting the fault plane, through downtown Los Angeles and into the San Gabriel Mountains. The three-dimensional structure along this traverse is shown in the lower right-hand quadrant in Figure 4a. The 115-km-long profile C-D (Fig. 1b) is along the axis of the Los Angeles basin but extends beyond either side of the basin. Profile C-D starts near Thousand Oaks and ends in Irvine, passing through the cities of Santa Monica, Inglewood, Compton, Garden Grove, and Anaheim. The three-dimensional structure along the C-D traverse is shown in the lower right-hand quadrant in Figure 4b.

There is an obvious correlation between the Los Angeles basin and the amplitude and duration of all the components of ground motion. As seen in the 118° record section (Fig. 4a), the direct *S* wave moves out from the fault (note the reversed polarity of the *S* wave at the fault near 21 km) and suddenly decreases in amplitude at about 50 km as it reaches the northern edge of the basin. The *S* wave continues to propagate into the medium outside the basin and with a higher velocity evidenced by the higher apparent velocity of the *S*-wave pulse. The effect of the basin can be seen by comparing the time histories in Figure 4a for distances less than 21 km, southwest of the fault, with the time histories at distances greater than 21 km. The medium southwest of the fault is the 1D approximation of the southern California crust. The structure of the basin and the lower seismic velocities in the basin have amplified and prolonged the ground motion significantly. In particular, the amplitude of the horizontal (28°) ground motion at 30 to 50 km and 60 sec into the record equals or exceeds the amplitude of the ground motion closest to the fault for the frequency range in our

simulations (Fig. 4a). This region of 30 to 50 km is directly over the deeper part of the Los Angeles basin.

These relatively large-amplitude phases (marked by *L* in Figs. 4a and 4b) are generated at the eastern and western boundaries of the basin. They originate around 30 to 40 km and 80 to 100 km on profile C-D (Fig. 4b) and slowly migrate with an apparent velocity of 1.0 to 1.5 km/sec into the deepest part of the basin arriving around 50 sec, as seen on the 28° record section A-B (Fig. 4a). Their predominant horizontal motion and their low apparent velocity suggest that they are Love waves. The time histories on profile C-D (Fig. 4b) also demonstrate the pronounced effect of the basin. Between about 24 and 95 km, the time histories show large amplitudes and long durations. The generation of these *L* waves is related to the steepness of the basin at its edges (Bard and Bouchon, 1980a, 1980b; Hill *et al.*, 1990) (Fig. 4b). Even though the low-velocity sediments extend beyond 100 km, the increased amplitude and duration is confined to distances less than 100 km where the sides of the basin are steep. This is particularly evident at the basin edge near Santa Monica—around a distance of 24 km along profile C-D (Fig. 4b). This abrupt end of the basin generates the largest *L* waves. On either side of the region between 24 and 95 km along profile C-D, a packet of *S* waves with duration of 10 sec or less propagates away from the basin with noticeably smaller amplitude.

While the deep Los Angeles basin continues to resonate, the waves pass through the shallower San Fernando basin with one exception. The deepest part of the San Fernando basin, northeast of the intersection of the I-5 and I-405 freeways, continues to vibrate well after the direct waves have passed, as seen in the snapshots at 40, 50, and 60 sec.

Elysian Park Earthquake

Since the 1987 Whittier Narrows earthquake, the Elysian Park thrust has emerged as one of the significant hazards for the Los Angeles metropolitan area (Davis *et al.*, 1989; Hauksson, 1990; Dolan *et al.*, 1995; WGCEP, 1995; Heaton *et al.*, 1995). We have selected one of the possible rupture areas capable of creating an *M* 6.7 earthquake on the Elysian Park thrust (Dolan *et al.*, 1995). The fault extends 16 km along a strike of 298° and dips 25° to the northeast for 21 km as it plunges from a depth of 10.5 km to a maximum depth of 19.0 km. The projection of the fault to the surface is shown as the rectangular area EP in Figure 1b. Geographically, this section of the Elysian Park thrust system lies directly below downtown Los Angeles, Pasadena, Glendale, and Hollywood. Structurally, it lies on the northern flank of the Los Angeles basin.

We model rupture on the Elysian Park as pure thrust with a hypocenter at a depth of 15 km midway along strike. Again, the rupture propagates radially outward with a velocity of 85% of the local shear-wave velocity. Due to the relatively shallow dip of the fault (25°), the component of motion perpendicular to the fault plane will produce significant vertical motion; this motion is reinforced by the direc-

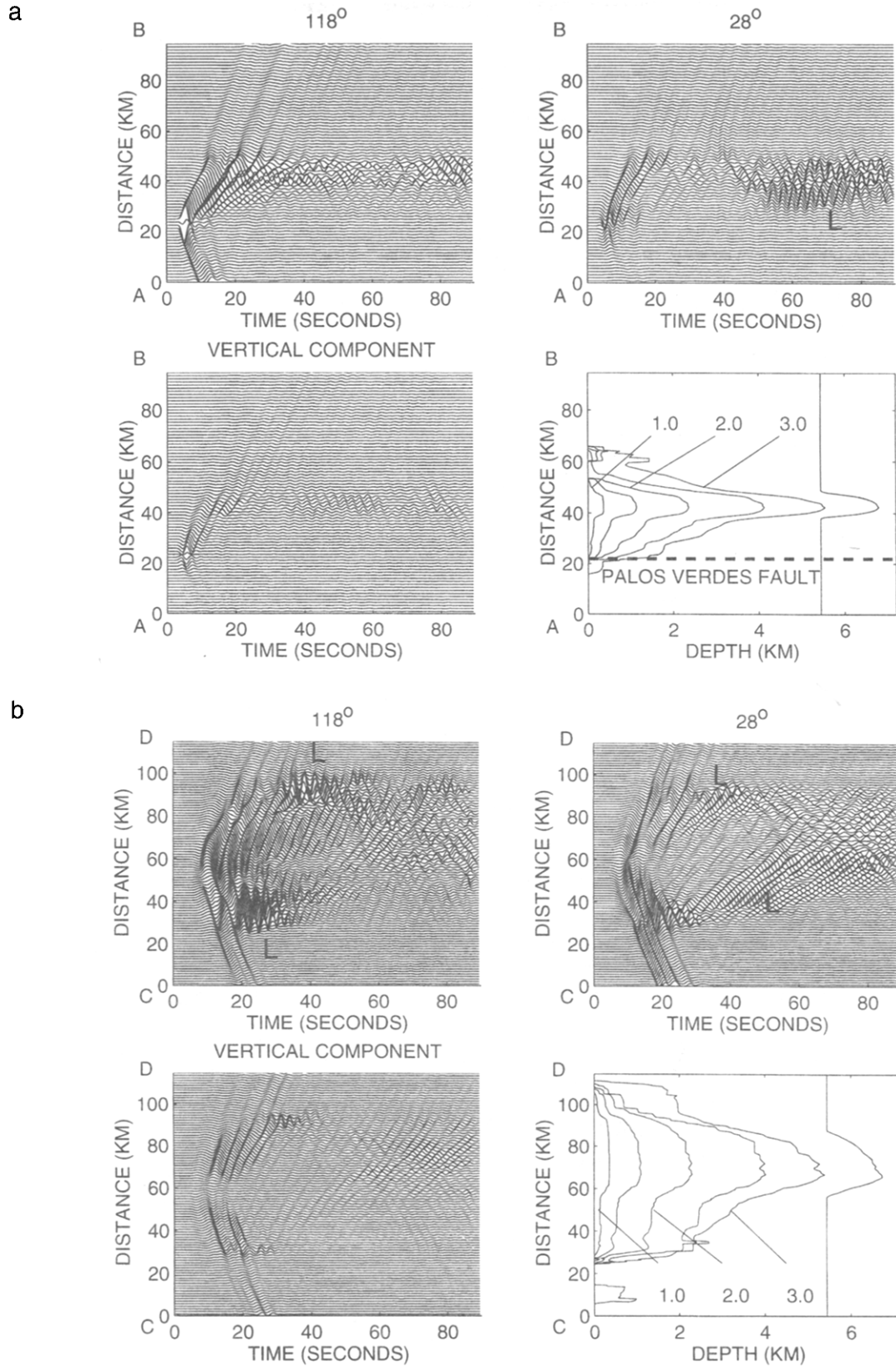


Figure 4. Simulated velocity seismograms along 118° and 28° and vertical for a constant-slip rupture on the Palos Verdes fault. The seismograms are for sites along profiles (a) A-B and (b) C-D (see Fig. 1b). *L* depicts basin-edge-induced waves. The lower right-hand quadrant shows a cross section of the *S*-wave velocity along each profile. Contour interval is 0.5 km/sec.

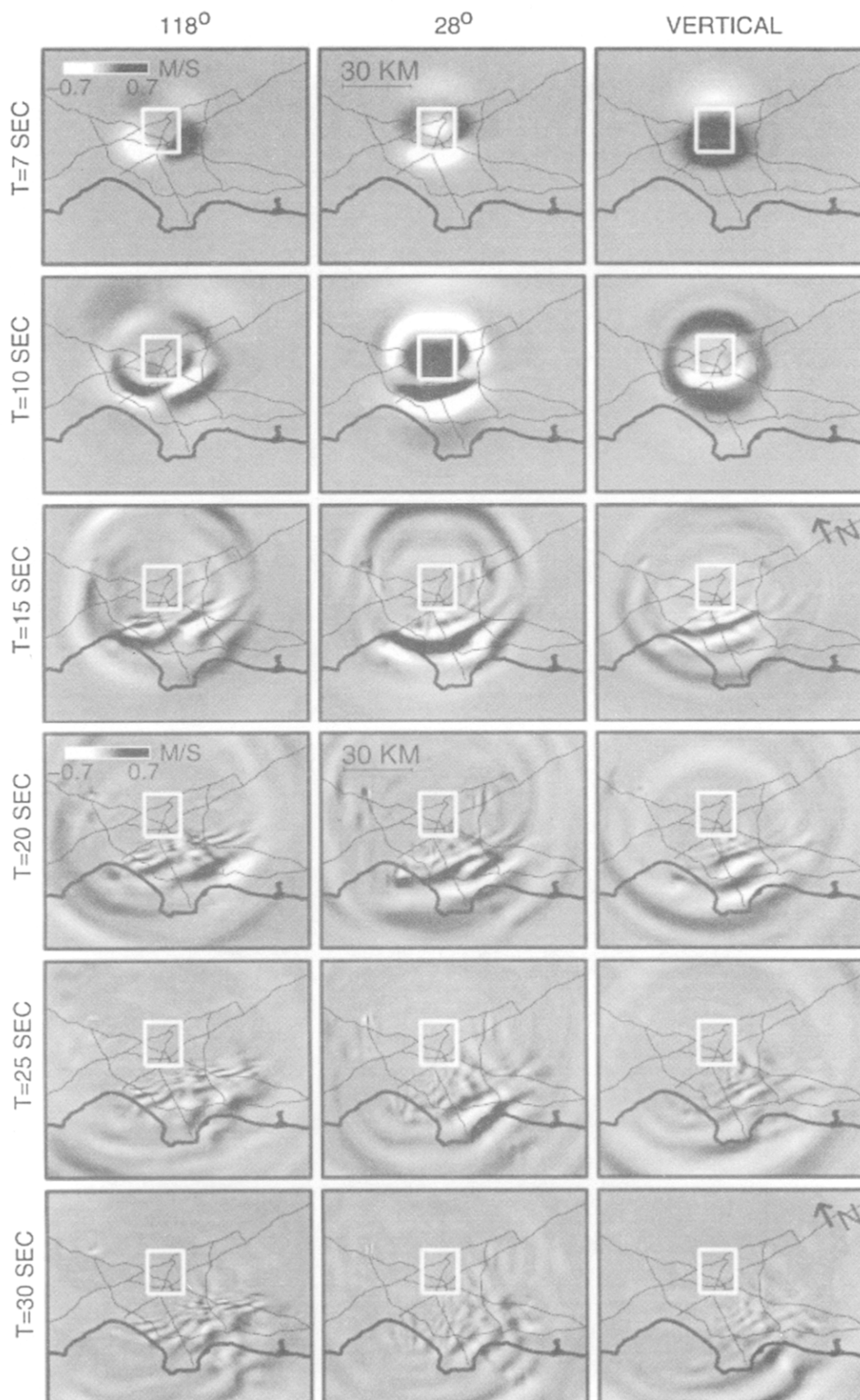


Figure 5. Same as Figure 3, but for a constant-slip rupture on the Elysian Park fault.

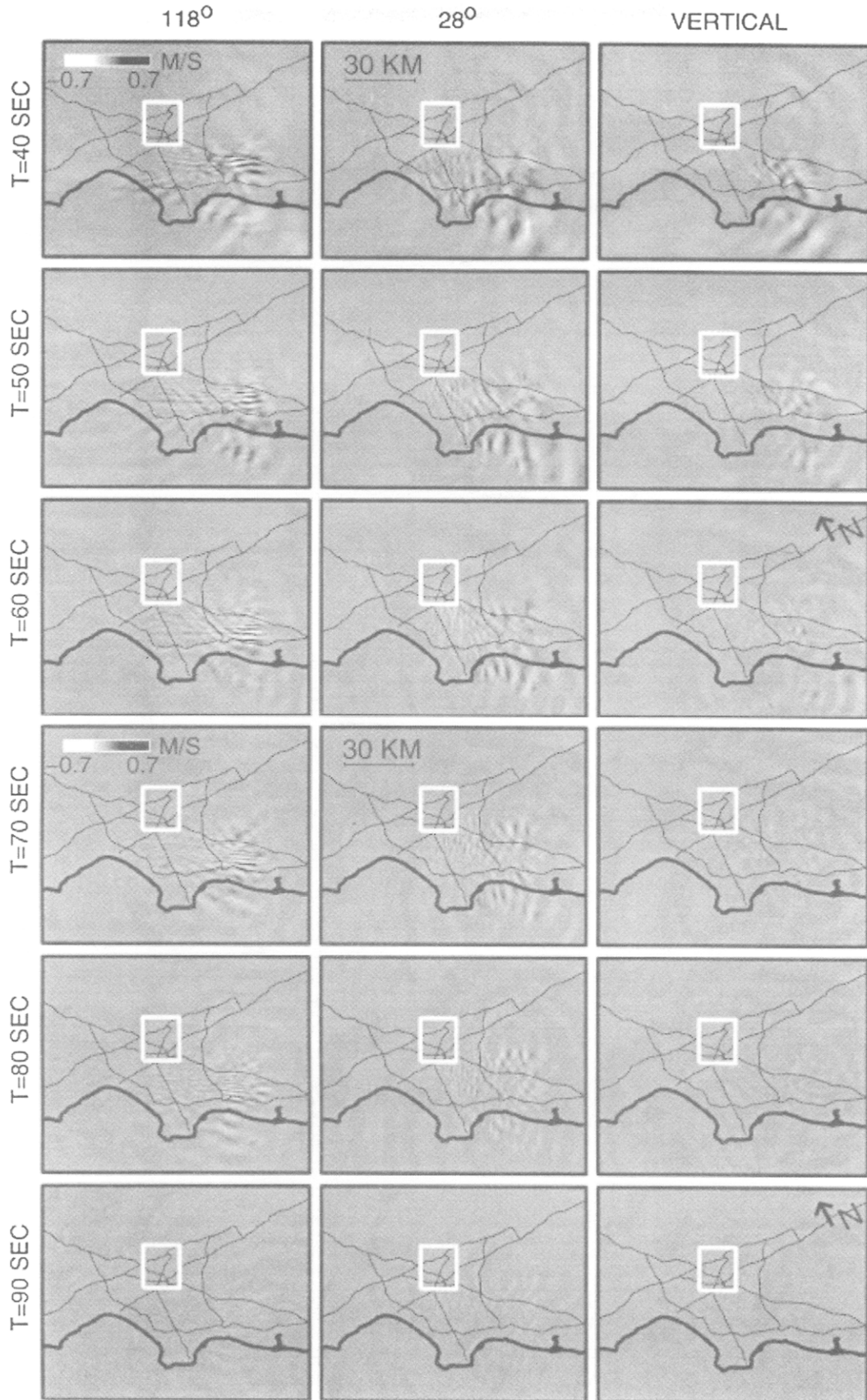


Figure 5. Continued

tivity of the thrust rupture mechanism (e.g., Archuleta and Hartzell, 1981; Heaton *et al.*, 1995). The slip itself produces the largest motions on the component along 28° . Thus, we expect that the horizontal component and the vertical component will produce the most intense ground motion.

In Figure 5, we show areal snapshots of the three components of ground motion radiating into the Los Angeles area. At 7 sec, the wave field is well developed with the updip directivity clearly established—note the intensity of the ground motion to the southwest compared with the northeast. This difference in amplitude of the ground motion is evident in all three components of motion. The 118° component has a well-developed four-lobed pattern with maximum amplitudes updip. The 28° component has the expected polarization for the thrust component, which rapidly reverses itself from 7 to 10 sec. Similarly, the vertical component, almost everywhere positive except for the region beyond the downdip extension of the fault, reverses polarity as the stopping phases arrive from the fault. By 15 sec, the Los Angeles basin is affecting the *S* waves; by 20 sec, the basin-generated waves are gaining strength, though the direct *S* waves are beyond the basin. Waves radiated northwest and northeast of the fault maintain circular wave fronts; waves radiated into the Los Angeles basin are distorted. Even though the vertical motion is pronounced in the first 30 sec, the horizontal motion dominates at later times. While the area immediately above the fault is relatively inactive by 25 sec, the main Los Angeles trough experiences significant shaking until 80 sec, especially in the area near the cities of Long Beach, Anaheim, and Santa Ana—the southeast end of the trough bounded approximately by the I-5 and I-405 freeways. The one other area experiencing significant shaking is the offshore region between the Port of Los Angeles and Huntington Beach; note snapshots at 30 to 80 sec.

We use profiles A-B and C-D (Fig. 1b) to illustrate the effect of the basin. Profile A-B crosses the eastern side of the surface projection of the buried fault; the profile crosses the updip edge of the fault projection at 47 km and the downdip edge at 68 km. The effect of directivity is immediately obvious comparing the amplitude of the 28° and vertical seismograms for distances 30 to 50 km with those for distances 65 to 85 km (Fig. 6a). Some of the difference in the amplitudes results from the impedance contrast between basin sediments (30- to 50-km range) and the normal southern California crust (distances greater than 65 km). The effect of the basin is certainly seen in the prolonged duration of the shaking in the distance range 25 to 50 km as compared with distances greater than 65 km.

The basin effect is even more clear in the C-D profile (Fig. 6b). Intense shaking throughout the basin lasts for about 20 sec. The steep edges of the basin around 30 and 90 km generate and trap large-amplitude basin waves (marked by *L* in Fig. 6b). These large amplitudes are primarily polarized along the $\pm 118^\circ$, corresponding to the long axis of the Los Angeles trough. The southeastern part of the basin (60- to 90-km range) experiences the most prolonged shak-

ing, about 80 sec, with an intensity slightly less than that near the fault. This area, near the Los Angeles–Orange county border, is the same area where the Palos Verdes earthquake produced shaking with large amplitudes and long duration.

Northridge Earthquake

The M 6.7 Northridge earthquake of 17 January 1994 is similar to the hypothetical rupture on the Elysian Park fault, but there are significant differences, especially the location (Fig. 1b). The rupture occurred on the northern edge of the San Fernando basin with directivity to the north, northwest. Our simulation of the Northridge earthquake using a simple approximation to the kinematic rupture is not an attempt to find a faulting model that “best fits” the data. In our frequency range 0 to 0.4 Hz (shortest wavelength is 2.5 km, but longer at depth where the elastic velocities are greater), we can only simulate gross features of the rupture process. By comparing synthetic time histories with data from the Northridge earthquake, we can examine which aspects of the 3D wave propagation are robust. For example, we can compare the distribution of peak velocities, the duration of shaking, and the partitioning of energy among the three components. Of course, the simulated Northridge earthquake also allows us to compare its ground motion with that from the Palos Verdes and Elysian Park earthquake simulations.

We approximate the Northridge earthquake as oblique slip (rake angle 101°) on a fault dipping 40° to the southwest and striking 118° (from Wald *et al.*, 1995, who used a strike of 122°). The fault is 18-km along strike and 22-km downdip. The rupture initiates at 18.5 km, propagates updip, and terminates at a depth of 6 km. Inversions of the strong-motion data (Wald *et al.*, 1995; Cotton *et al.*, 1995) show a heterogeneous distribution of slip on the fault. However, since our computed long-period ground motion is somewhat insensitive to such small-scale variations in the slip, and to enable comparisons with the other simulations, we have kept the rupture kinematics the same. A major difference with the Northridge earthquake is the direction of rupture propagation: the rupture progresses away from the greater Los Angeles area. Nonetheless, the ground motion in the Los Angeles basin shows similarities to the other two simulated earthquakes.

We show snapshots of the ground motion at 20, 40, and 80 sec to highlight the interesting features (Fig. 7). In the early stages of the rupture, the spatial distribution of the radiated ground motion near the fault is similar to that for the Elysian Park earthquake. The 28° horizontal and vertical motions are dominant and show the effects of directivity. However, around 15 sec near the northwest corner of the fault, the deepest part of the San Fernando basin (Fig. 1c) begins to act like a secondary source—note how the waves are centered on this point in the snapshot at 20 sec (Fig. 7). The fault never actually ruptures into these sediments, which penetrate to a depth of 4.5 km, but terminates just below this

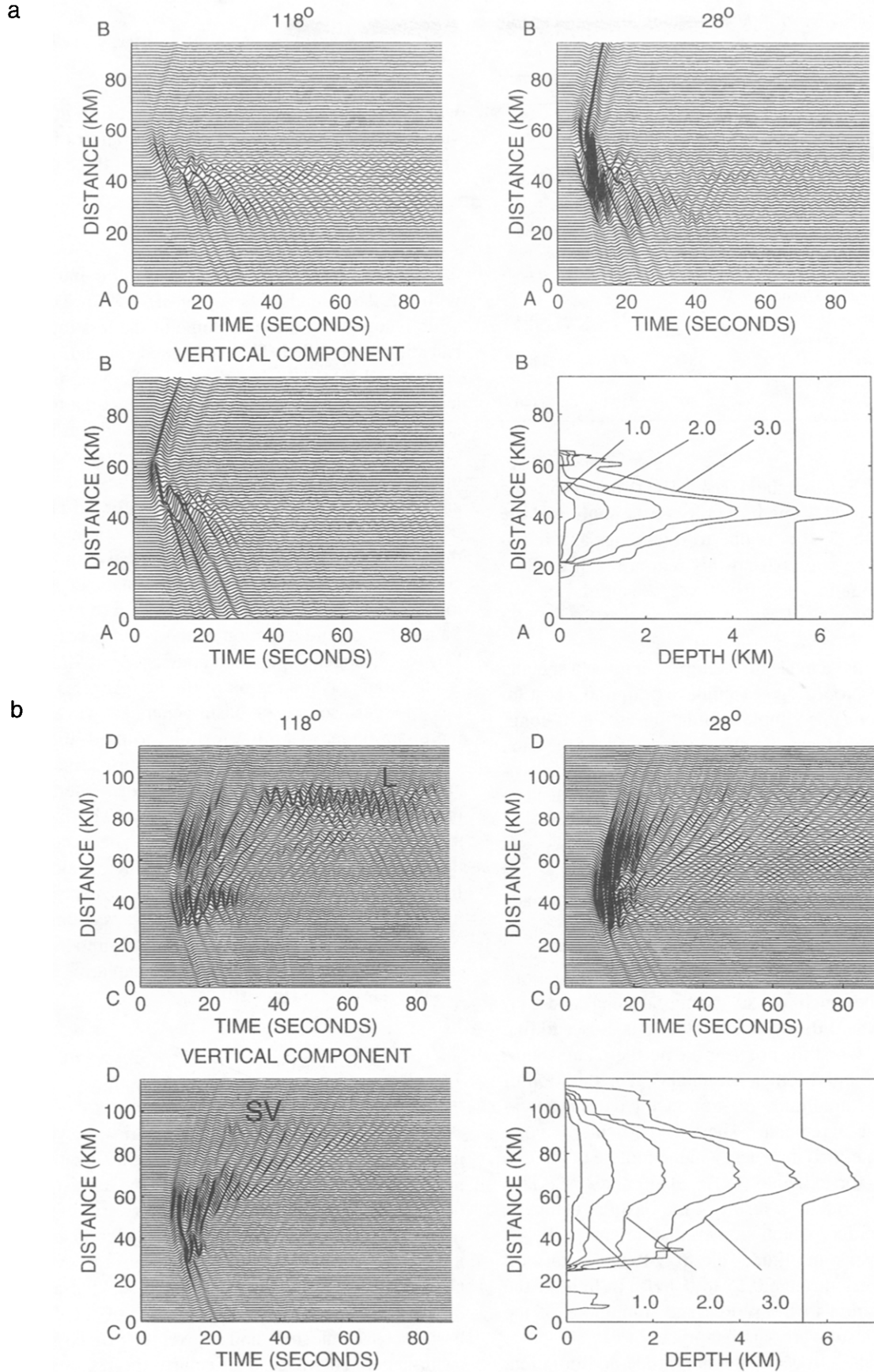


Figure 6. Same as Figure 4, but for a constant-slip rupture on the Elysian Park fault. The seismic amplitudes are directly comparable to those shown in Figure 4.

Table 3
Maximum Peak Velocities and Cumulative Kinetic Energies

Component	Ground-Motion Parameter	Simulation		
		Palos Verdes	Elysian Park	Northridge
118°	peak particle velocity (m/sec)	0.40	0.32	0.22
28°	peak particle velocity (m/sec)	0.44	0.67	0.58
Vertical	peak particle velocity (m/sec)	0.16	0.25	0.46
118°	cumulative kinetic energy (J-s)	911	192	144
28°	cumulative kinetic energy (J-s)	584	671	1407
Vertical	cumulative kinetic energy (J-s)	50	124	440

deepest part of the San Fernando basin. The strong resonance in this basin is caused by its proximity to the fault, and the amplification of the waves is due to directivity and impedance contrast. The waves from this region reach the Los Angeles basin around 25 sec. By 40 sec, the entire Los Angeles basin is fully excited, and shaking persists through 80 sec (Fig. 7).

Although we have made no attempt to impose a specific slip model for the Northridge earthquake or to find a best fit, the synthetics from this simple simulation, given its long-period nature, should resemble the gross features of the data. To compare data from the Northridge earthquake with synthetic time histories, we have bandpass-filtered both the data and the synthetics to their common frequency band 0.15 to 0.4 Hz. In Figure 8, we show a comparison between data and synthetics for 12 stations representing various azimuths and distances. For each station, the comparisons are made at the same scale for all three components and for the available record length of the data. The fit among the phases varies significantly. The best results are obtained for stations located at rock sites such as SSA (Santa Susanna) and GPK (Griffith Park), where the surficial velocity is closer to that in the model. The worst fits are near the northern and southern edges of the Santa Monica Mountains. The duration of the signal and the amplitude of motion for data and synthetics are in fair agreement. There is particularly good agreement with late-arriving energy in the middle of the Los Angeles trough—for example, DOW, BAP, and LAS. This energy is almost certainly a result of the basin structure as opposed to the source, which stops radiating energy by 15 sec. Most of the peak amplitudes are fit within a factor of 2 (Fig. 9) for this period range 0.15 to 0.4 Hz. In light of the simple approximation to the source and limitations of the basin model, the results are satisfactory.

To combine the effects of the amplitude and duration, we use the total cumulative energy E_{tot} in the seismograms. For each grid point (x, y) on the surface, we have computed the cumulative energy for each component of motion:

$$E_k(x, y) = \frac{1}{2} \rho(x, y) \int_0^T \dot{u}^2(x, y, t) dt,$$

where k is the component, ρ is the density, $\dot{u}(x, y, t)$ is the velocity seismogram, and T is the duration of the seismogram. The total energy is the sum of all three components:

$$E_{\text{tot}}(x, y) = E_{118}(x, y) + E_{28}(x, y) + E_v(x, y)$$

Figure 10 shows a map of the total cumulative energy with the isoseismals (Dewey *et al.*, 1995). The amplitude scale is logarithmic so that some of the less intense regions can still be identified. There is a good correlation of the total energy and MMI VIII isoseismal in the area directly above and to the north of the fault. This is the area most strongly affected by directivity of the rupture as well as being closest to the fault plane. The maximum cumulative energy is attained above the northeast corner of the fault, which is an area with a large concentration of unsafe (red-tagged) buildings (OES Map DR-1008, 1994). The region just south of the 101 freeway within the MMI VIII isoseismal is not well correlated with the total cumulative kinetic energy—a point to be discussed later. With the exception of two small areas, Santa Monica and a section of the I-10 freeway, the greater Los Angeles area experienced intensities of MMI VII or less. Santa Monica is the region of the Los Angeles basin that is the strongest source of basin-generated waves. Note that there is a finger of MMI V parallel to the I-405 that nearly coincides with the region of smaller cumulative energy. The cumulative energy would suggest higher intensities within the broad MMI V region of the basin. The maximum cumulative energy within the Los Angeles basin coincides with the area near the I-605 freeway near Lakewood, California. In fact, there are MMI VI intensities in the central part of the basin between the I-5 and I-405 freeways ending at the city of Anaheim (Dewey *et al.*, 1995). Anaheim is very near the southeast end of the region of high cumulative energy in the Los Angeles basin (Fig. 10).

Comparison of the Ground Motion for the Three Earthquakes

While the three earthquake scenarios are very different from one another, there are some generalizations. As expected, the areas near the fault have the largest ground motions, especially those areas in the forward direction of the rupture. The style of faulting makes a significant difference in the ground-motion pattern. The deep Los Angeles basin profoundly increases the duration of shaking and, in some areas, the amplitude. The steep sides of the Los Angeles basin act as reflectors and are regions of large-amplitude basin-generated waves, particularly the regions near Santa Monica and along the I-5 freeway between downtown Los Angeles and Anaheim (Fig. 1b).

To illustrate these effects, we show the spatial distri-

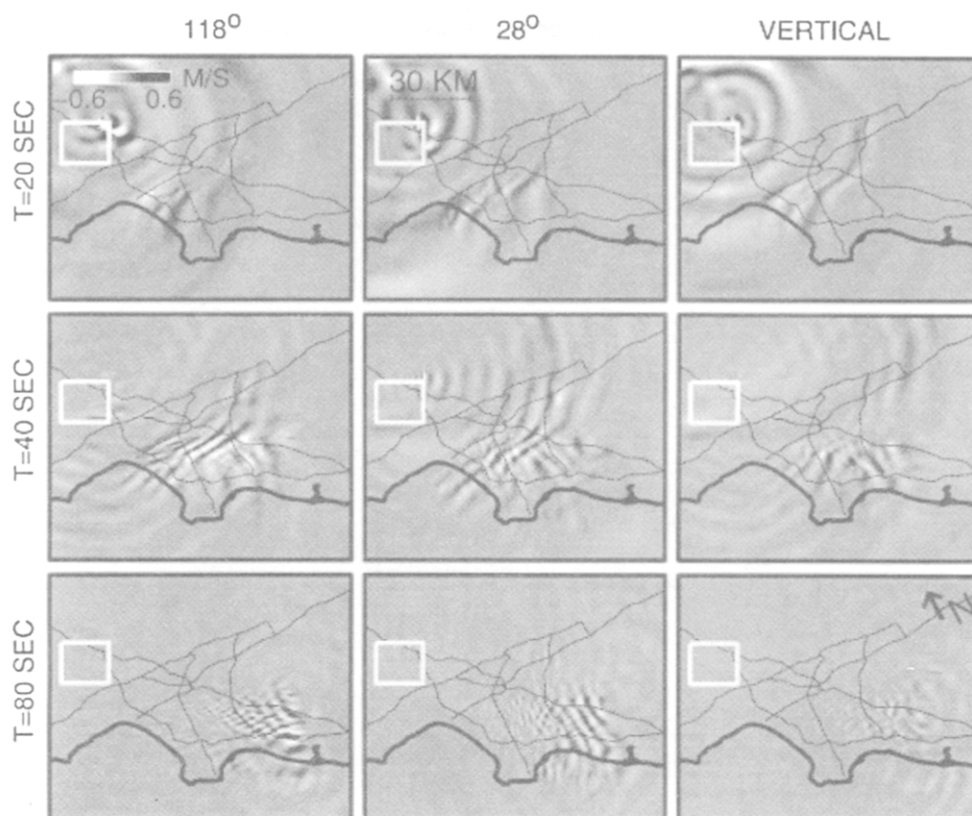


Figure 7. Snapshots of simulated wave propagation in the Los Angeles area for a constant-slip rupture on the Oak Ridge fault (Northridge); the snapshots depict velocities along 118° and 28° and vertical at 20, 40, and 80 sec after the origin time of the rupture. For explanation, see Figure 3.

bution of the cumulative kinetic energy for each component of motion for each earthquake (Fig. 11). The cumulative energy scale is the same for all three earthquakes. The deep blue (red) represents the minimum (maximum) cumulative energy. The strike-slip Palos Verdes fault shows the classic bow-tie pattern on the fault-perpendicular (28°) component that is strongly affected by the directivity (Archuleta and Frazier, 1978; Archuleta and Hartzell, 1981). The fault-parallel component (118°) has significant energy near the fault. In part, this energy comes from the large slip in the sediments, but it also results from the directivity as the rupture propagates from depth to the surface. What is surprising is the large amount of energy in the main part of the Los Angeles basin and also near the base of the Santa Monica Mountains. The former is surprising in that the energy would normally be decreasing with distance; however, the increased amplification above the deepest parts of the basin is consistent with the results from other 3D basin studies (e.g., Olsen *et al.*, 1995a, 1996). The latter is surprising because the area near Santa Monica is nearly nodal for strike-slip faulting on the Palos Verdes fault. It is not simply a source effect because the bilateral symmetry does not produce a similar feature at the southeast end of the rupture. This region near the Santa Monica Mountains is a source for basin-

edge-generated waves (Figs. 4 and 5). The largest value of cumulative energy occurs here with a value of 911 J-s. Of the three simulated earthquakes, the Palos Verdes simulation produces the broadest high-level areal cumulative kinetic energy. In part, this is because slip occurs at shallow levels and therefore promotes the generation of surface waves. The fault geometry and rupture direction of the Palos Verdes earthquake is directing significant energy into the region near Santa Monica—the most effective source of basin-edge-generated waves. Once generated, these waves propagate southeastward along the main trough of the Los Angeles basin, prolonging the duration of shaking.

Although the simulated Elysian Park earthquake is quite similar to the Northridge earthquake, the ground motion in the region around the projection of the fault at the Earth's surface is very different. Most of this difference can be explained by the rupture directions for the two earthquakes: the Elysian Park rupture is updip into the sediments of the Los Angeles basin (surface shear-wave velocity of 1.0 km/sec), while the Northridge rupture is updip away from the Los Angeles basin into rock (surface shear-wave velocity of 3.06 km/sec). Thus the seismic energy for the Elysian Park event is amplified by both the directivity of the rupture and the impedance contrast of the sediments relative to base-

OBSERVED VS SYNTHETIC VELOCITY SEISMOGRAMS 0.15–0.4 HZ

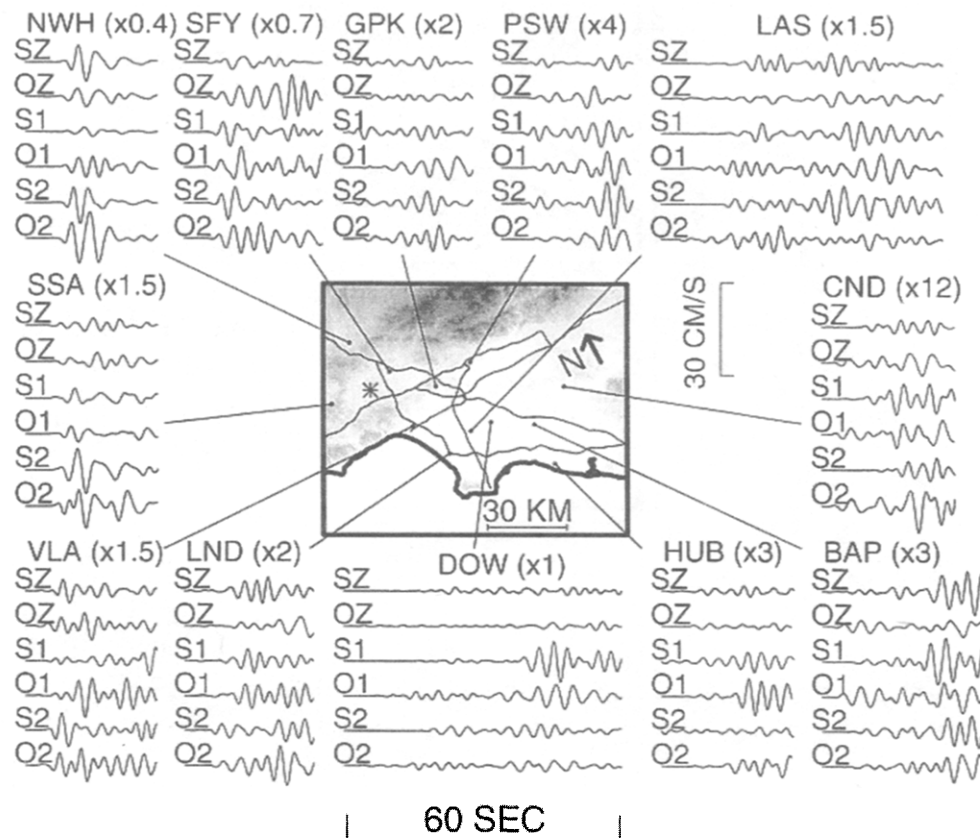


Figure 8. Comparison of simulated and observed 0.15 to 0.4-Hz velocity seismograms for the 17 January 1994 Northridge event at 12 recording sites in the Los Angeles region: horizontal components 118° (1) and 28° (2) and vertical component (Z). S denotes the synthetic seismograms, and O denotes the observed seismograms. Amplitude scaling factors listed at the station abbreviation have been applied to each pair of simulated and observed seismograms. The epicenter for the Northridge event is shown by the asterisk on the topographic map. The thin lines are major freeways in the Los Angeles area (Fig. 1b).

ment, a factor of 2.3. The Elysian Park earthquake shows a much broader area of energy ahead of the updip projection of the fault compared to that for the Northridge event (compare both the 118° and 28° cumulative energy plots in Fig. 11). The maximum cumulative energy is 671 J-s almost in the center of the 28° lobe southwest of the fault's surface projection. It is interesting to see the asymmetry of the cumulative energy on the 118° component for the Elysian Park simulation. Recall that this component is approximately parallel to the axis of the Los Angeles basin. There is a large lobe of cumulative energy to the southeast, in the main trough of the basin, compared with the southwest; the 28° component is rather symmetrical. In all of the simulations, the main trough of the Los Angeles basin is easily discernible in these plots of cumulative kinetic energy. To a large degree, this is due to the prolonged duration of the shaking caused by the basin itself.

The one area where Northridge produces the maximum cumulative energy (and its maximum particle velocity) is

where the fault stops beneath the deepest part of the San Fernando basin. This is the same region discussed earlier as acting like a secondary source during the Northridge simulation. In fact, this deep trough produces the largest cumulative energy, 1407 J-s on the 28° component, of any of the simulated earthquakes (Table 3). Northridge produces significant energy on the vertical component as well with a maximum of 440 J-s collocated with the 28° maximum. Part of the explanation for this large vertical motion derives from the dip of the fault (40°) and part from the velocity structure. The more competent material of the Santa Susanna Mountains north of the Northridge fault will only slightly turn the ray path of SV waves toward the vertical, thus maintaining its projection of its amplitude onto the vertical component. For the Elysian Park simulation, where the waves are traveling into the sediments, the opposite occurs. Thus there is less vertical and more horizontal motion due to the SV waves.

Besides the deepest part of the San Fernando basin, evident in all three earthquake simulations—note the bright red

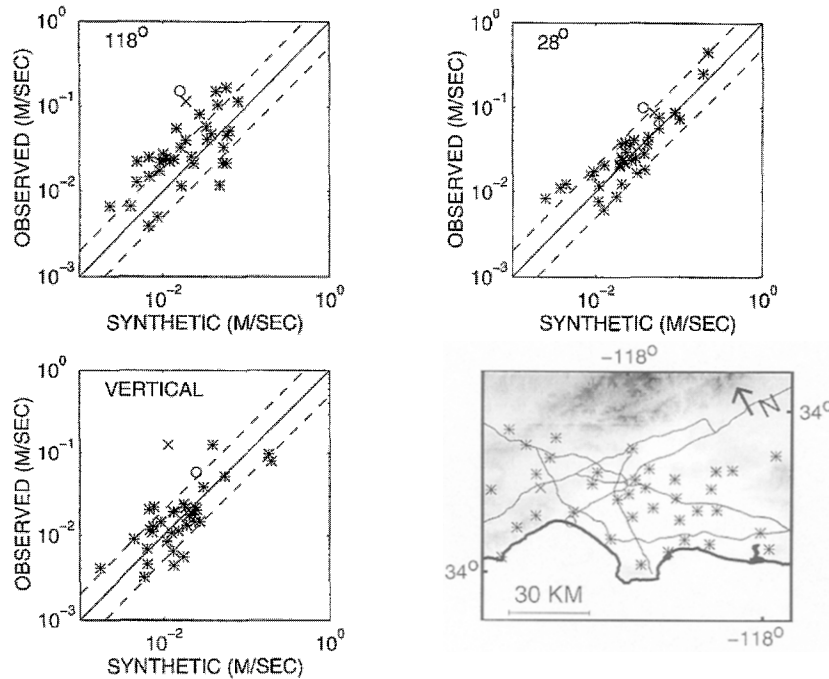


Figure 9. Graphs of observed versus 3D simulated peak velocities for the 17 January 1994 Northridge event. The values shown are for 38 different sites in the Los Angeles area (see map). Peak velocities and locations for recording stations Tarzana (TAR) and Santa Monica City Hall Grounds (SMG) are shown by “x” and “o,” respectively; all other peak velocities and locations are shown by asterisks. The dashed lines represent factor-of-2 discrepancies between the observed and simulated peak velocities. The thin lines on the map show major freeways in the Los Angeles area.

area in the northwest quadrant (Fig. 11), the other area that is very noticeable is the offshore area. The increased amplification in this region is most prominent for the Palos Verdes and Elysian Park simulations. This offshore sub-basin (Fig. 1c) traps the seismic waves and prolongs their duration of shaking much like the deepest part of the San Fernando basin.

The peak particle velocity has to be taken in the context of the frequency range of the simulations, 0.0 to 0.4 Hz. The maximum particle velocities are 0.44, 0.67, and 0.58 m/sec for the Palos Verdes, Elysian Park, and Northridge simulations, respectively (Table 3). Given the limited frequency range, the computed peak velocity is a lower bound for earthquakes of this size. In all cases, the maximum velocity occurred on the 28° component—the component most affected by directivity. The patterns of particle velocity are nearly coincident with those for cumulative energy (Fig. 11).

The proximity of the faulted area to the Earth’s surface is a major factor. The Palos Verdes fault ruptures within 0.5 km of the surface; Elysian Park stops at 10.5 km, and Northridge stops at 6.0 km from the Earth’s surface. Even though the Elysian Park rupture is almost twice as far from the Earth’s surface, it produces about the same peak velocity as the Northridge rupture. As discussed above, the most probable reason is that the Elysian Park rupture is directed into the sediments that amplify the ground motion, while the Northridge rupture is directed into rock.

Discussion

Although the 1994 Northridge earthquake demonstrated just how devastating an earthquake could be in southern California, direct comparison of the ground motion from three

simulations shows that larger areas of the metropolis will experience much more intense ground shaking from similar magnitude earthquakes on either the Palos Verdes or Elysian Park faults. While the proximity of the Palos Verdes and Elysian Park faults to the metropolitan area is a principal factor, the interaction between the 3D structure and the faulting significantly affects the ground motion.

A similar finite rupture model for the Elysian Park fault embedded within a 1D velocity structure was analyzed by Heaton *et al.* (1995). They considered a fault with a dip of 23°, length 35 km, downdip width 18 km, and a strike of 270°. Faulting was confined to depths between 9 and 16 km. The slip and rise time were variable everywhere on the fault; average slip was 2.2 m, producing a M_w 7.0 earthquake. The computed ground motion was limited to frequencies less than 1.0 Hz. They computed the ground motion on an 11 × 11 surface grid with 5-km spacing. Because of the variable slip and rise time, it is difficult to compare directly their results with ours. However, the directivity and the amplification due to the sediments are well documented in both models. A major difference is that their lobe of maximum velocity is within the fault’s projection to the surface; of course, the shape of the contours are elongated in the direction of rupture propagation and extend beyond the fault’s projection. A second major difference is the duration of the signal; they anticipated signal durations less than half of what would occur if a 3D basin model were used.

The relatively strong and coherent Love waves that emerge at the steep basin edges, especially notable for the Palos Verdes earthquake, are in general agreement with results from simulations of wave propagation in basin models (e.g., Bard and Bouchon, 1980a; Vidale and Helmberger, 1988; Hill *et al.*, 1990; Olsen and Schuster, 1992; Frankel

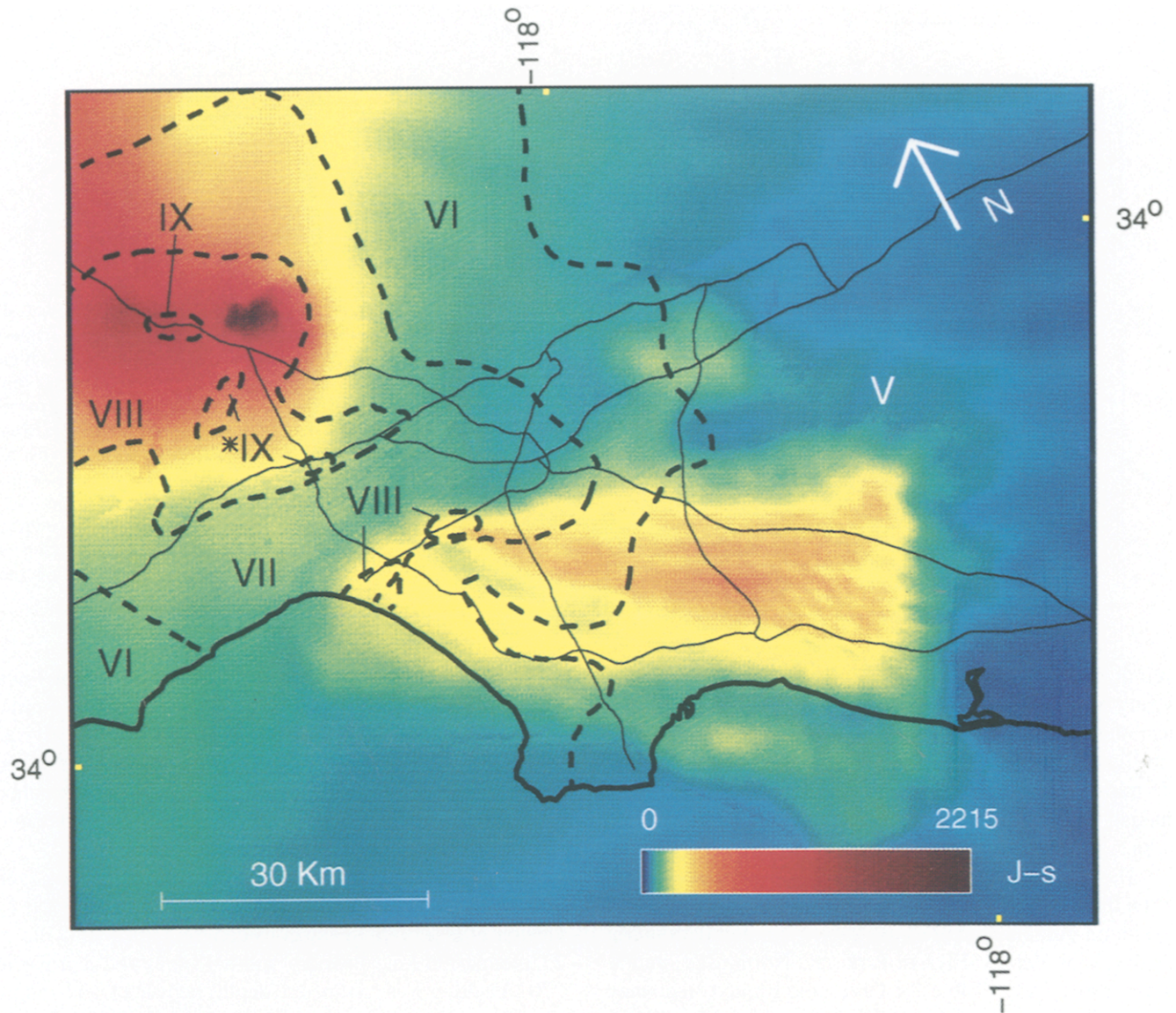


Figure 10. Map of simulated total cumulative kinetic energies for simulation of the M 6.7 Northridge event. Note that the color scale is logarithmic. The thick dashed lines depict the boundaries of modified Mercalli Intensity zones V-IX (Dewey, 1995). The thin lines show major freeways in the Los Angeles area. The thick solid line is the coastline. The epicenter for the Northridge event is shown by an asterisk.

and Vidale, 1992; Yomogida and Etgen, 1993; Olsen and Schuster, 1994; Olsen *et al.*, 1995b). However, the 3D structure coupled with a propagating rupture on faults with different geometry highlight the large variability of the ground motion for earthquakes with the same seismic moment. It is clear that the steep edge of the basin near Santa Monica plays a pivotal role in generating basin waves (Figs. 4 and 5). This steep edge of the basin certainly could be a contributing factor to the localized damage in this area during the Northridge earthquake (Gao *et al.*, 1996). However, this is one of the areas where our simple simulation of the Northridge earthquake severely underpredicted the amplitude of the ground velocity.

While we made no attempt to use a specific model of the Northridge event, such as Wald *et al.* (1996), the simulated ground velocity generally agreed within a factor of 2 for most of the stations. The primary areas of disagreement were near the edges of the Santa Monica Mountains, both Santa Monica and Sherman Oaks. Graves (1995) found that he could more accurately model the *SH* ground velocity at Santa Monica if he added a small localized microbasin to a more general Los Angeles basin model. It would be numerically impossible for us to add such small-scale features with low velocities into our 3D regional model. Nonetheless, Graves's result points out that very local site effects can strongly affect the amplitude of the ground motion. One of

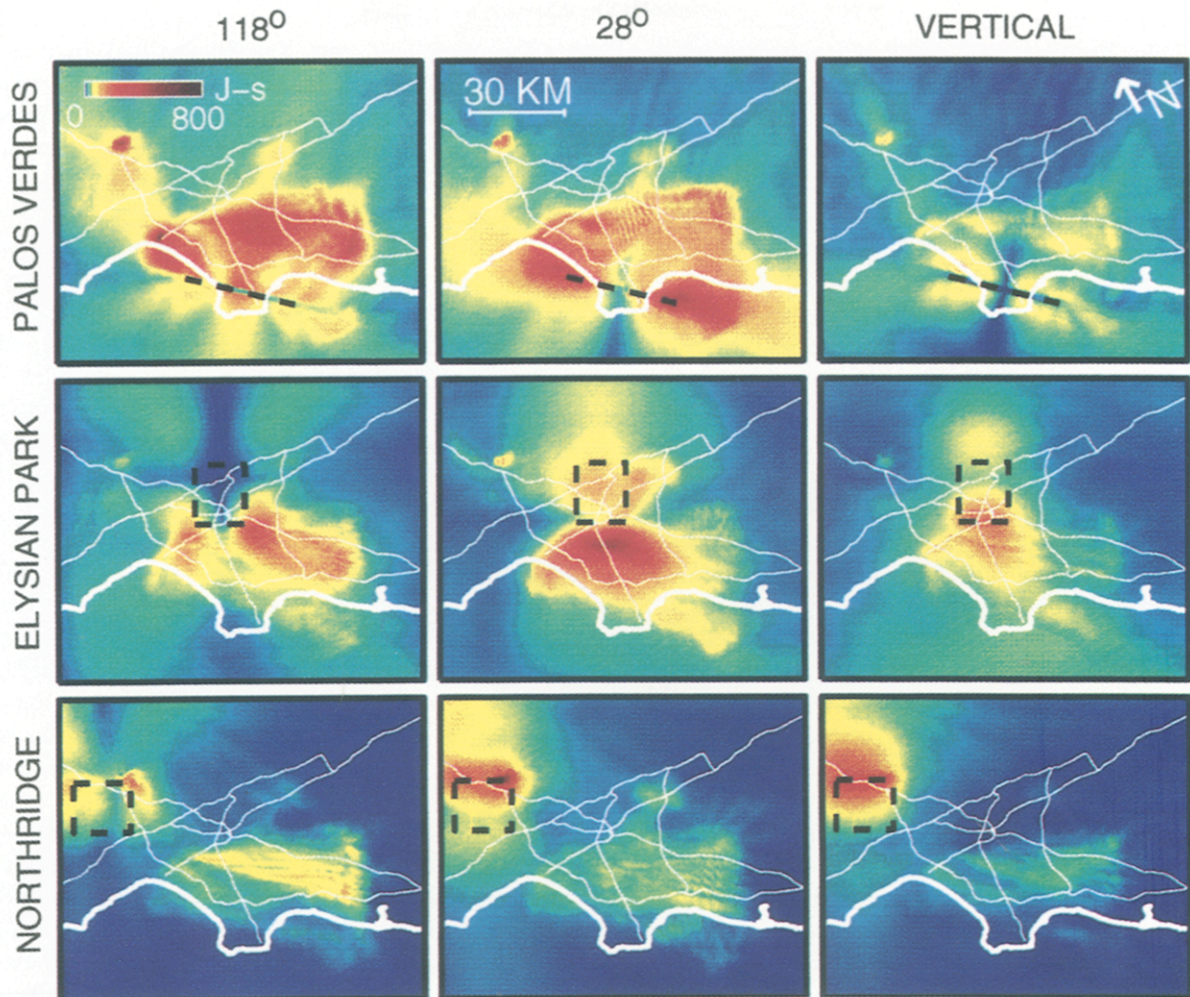


Figure 11. Maps of simulated cumulative kinetic energies for hypothetical constant-slip M 6.75 ruptures on the Palos Verdes and Elysian Park faults and for the M 6.7 rupture on the Oak Ridge fault (Northridge). The cumulative kinetic energies are shown along 118° and 28° and vertical. Note that the color scale is logarithmic and covers values between 0 and 800 J-s for all three simulations. The thick, dashed lines depict the surface projections of the faults. The thin white lines show major freeways in the Los Angeles area. The thick white line is the coastline.

the major limitations of this study is that the near-surface shear-wave velocity is capped at 1.0 km/sec, for computational feasibility, and does not take into account the surficial lower velocities (<0.5 km/sec; see, for example, Fumal *et al.*, 1980) in the Los Angeles basin. It is possible that the omission of the near-surface low-velocity layer is in part responsible for underpredicting the cumulative kinetic energy just south of the 101 freeway (Fig. 10). The primary effects of capping the shear-wave velocity is that the simulations probably underestimate the overall amplitude and in particular the duration (e.g., Olsen *et al.*, 1995a, 1996). These effects may be partially compensated for because we have not included attenuation in the model. Thus, if we expect lower surficial velocities to amplify the ground motion, adding lower Q values will attenuate the ground motion. Frankel and Vidale (1992), Frankel (1993), and Olsen *et al.*

(1995a, 1996) showed that attenuation can be a major limiting factor to the duration of shaking in alluvial valleys. However, comparing synthetics and data for Northridge shows that both the amplitude and the duration are quite well modeled (Figs. 8 and 9); thus, for the frequency band 0 to 0.4 Hz, the near-surface velocity and attenuation are apparently not systematically affecting our results.

The simulations reflect the broadscale basin effects coupled with the particular earthquake geometry. The seismic radiation pattern expected from each faulting style is distinguishable, but the symmetry is clearly distorted by the 3D velocity structure. The Los Angeles basin increases the size of the area that experiences significant shaking, e.g., the 118° component for the Elysian Park earthquake (Fig. 11). Although the Palos Verdes simulation does not produce the maximum peak velocity or peak cumulative energy, it af-

fects the most area—much of which is offshore (Fig. 11). Both the Palos Verdes and Elysian Park simulations produce significant ground motion in the Los Angeles basin; in particular, the Elysian Park simulation generates more intense amplitudes over shorter duration. The slip for the Elysian Park earthquake is confined to depths of more than 10 km. Obviously, if slip were allowed to come closer to the surface, like Northridge or the 1971 San Fernando earthquake, the intensity of shaking would be even greater. In all three simulations, the horizontal component (28°) produced the maximum particle velocity and is most affected by the directivity of the rupture.

The maximum peak particle velocities range from 0.44 to 0.67 m/sec for the three simulations. These peak motions are less than half of those predicted for a large (M 7.75) earthquake on the San Andreas fault near Los Angeles (Olsen *et al.*, 1995b). Realizing that the time histories are limited to frequencies less than 0.4 Hz and that the near-surface S -wave velocity is capped at 1.0 km/sec, we expect these values to be lower bounds to what can be expected in the near-source area (Archuleta and Hartzell, 1981; Heaton *et al.*, 1995). With more realistic surficial S -wave velocities and higher frequencies, the simulations of earthquakes on the Los Angeles fault system would almost certainly produce higher ground velocities; however, due to the attenuation of higher-frequency ground motion with distance from the fault, this may not be the case for the San Andreas rupture. Future simulations, including higher frequencies, more realistic near-surface velocities, and attenuation, are required to compare the hazards from earthquakes on the Los Angeles fault system and the San Andreas fault.

Conclusions

For the greater Los Angeles area ($10,925 \text{ km}^2$), we have computed 90 sec of ground shaking from three simulated earthquakes taking into account the 3D velocity structure and propagating slip over finite faults. The three earthquakes—Palos Verdes, Elysian Park, and Northridge—all have practically the same moment magnitude of M 6.7 to 6.75. Time histories of ground velocity in the frequency band 0.0 to 0.4 Hz are computed at 400-m grid spacing throughout the $95 \times 115 \text{ km}$ area. Naturally, the pattern of the ground motion is directly related to the style of faulting—strike slip for Palos Verdes, reverse for Elysian Park, and reverse-right lateral for Northridge—and the location of the fault. The ground motion is tightly coupled to the interaction between the 3D velocity structure and the style of faulting.

Love waves generated at the basin edges for the Palos Verdes earthquake and refracted S waves for the Elysian Park event maintain signal durations at some basin sites beyond 90 sec. The steep edge of the basin near the Santa Monica Mountains is particularly efficient for generating Love waves from the Palos Verdes earthquake. The southeasternmost edge of the basin near Anaheim and Santa Ana

traps energy in the basin and prolongs the duration of shaking for all of the events. The Elysian Park rupture directs energy into the Los Angeles basin sediments creating a broad region of intense shaking southwest of the fault's surface projection. The deepest part of the San Fernando basin acts like a separate source radiating its own waves even after the slip on the fault has healed.

Both the Palos Verdes and Elysian Park simulations produce intense ground motion in the Los Angeles basin. Even though the Palos Verdes earthquake ruptures almost to the Earth's surface, the Elysian Park earthquake, which is confined to a depth of more than 10 km, generates a larger peak velocity, 0.67 m/sec compared with 0.44 m/sec. Because of the geometry of these faulting scenarios, the rupture directivity always enhanced the 28° component of motion relative to the other two components.

The simple approximation of the Northridge earthquake reproduces the overall pattern of peak velocities in the Los Angeles area within a factor of 2. However, for sites in localized areas near the Santa Monica Mountains, the simulation significantly underpredicts the large observed horizontal peak motion. For sites outside these areas, comparison of synthetic velocity waveforms and data show fair to good correlation in both duration and peak values. The simulation generally predicts the amplitude and timing of late-arriving phases in the Los Angeles basin. The pattern of total cumulative kinetic energy generally matches that for the damage intensities in the San Fernando Valley. In the Los Angeles basin, there is some agreement with the MMI VI extending southeast over the main trough of the basin but less correlation for the more intensely damaged areas between the Santa Monica Mountains and north of the I-10 freeway.

Although the simulations give the distribution of ground velocity over the greater Los Angeles region, they are limited to low frequencies, 0 to 0.4 Hz. The simulations provide the gross distribution of ground motion resulting from the interaction of the faulting with the large-scale 3D structure of the area. The simulations demonstrate that the basin structure plays a pivotal role in the pattern and duration of the ground shaking. While Northridge may have been the most expensive earthquake in U.S. history, these simulations show that a similar size earthquake on the Los Angeles fault system produces even more severe ground shaking in the metropolitan areas.

Acknowledgments

We are grateful to G. T. Schuster for permitting us to use his SGI Powerchallenge supercomputer to carry out the 3D simulations. We give special thanks to H. Magistrale for allowing us to use his 3D Los Angeles basin model and to S. Day for valuable advice on insertion of the double-couple source into the finite-difference scheme. We thank A. Tumarkin, A. Frankel, J. Vidale, and J. Pechmann for their thoughtful comments, all leading to an improved article. This work was supported by the Southern California Earthquake Center (SCEC), USC 572726, through the NSF cooperative agreement EAR-8920136, ICS Contribution 0236-49EQ.

References

- Archuleta, R. J. and G. A. Frazier (1978). Three-dimensional numerical simulations of dynamic faulting in a half-space, *Bull. Seism. Soc. Am.* **68**, 541–572.
- Archuleta, R. J. and S. H. Hartzell (1981). Effects of fault finiteness on near-source ground motion, *Bull. Seism. Soc. Am.* **71**, 939–957.
- Archuleta, R. J. and S. M. Day (1980). Dynamic rupture in a layered medium: the 1966 Parkfield earthquake, *Bull. Seism. Soc. Am.* **70**, 671–689.
- Archuleta, R. J. (1984). A faulting model for the 1979 Imperial Valley earthquake, *J. Geophys. Res.* **89**, 4559–4585.
- Bard, P.-Y. and M. Bouchon (1980a). The seismic response of sediment-filled valleys. Part 1. The case of incident SH waves, *Bull. Seism. Soc. Am.* **70**, 1263–1286.
- Bard, P.-Y. and M. Bouchon (1980b). The seismic response of sediment-filled valleys. Part 2. The case of incident P-SV waves, *Bull. Seism. Soc. Am.* **70**, 1921–1941.
- Beroza, G. C. (1991). Near source modeling of the Loma Prieta earthquake: evidence for heterogeneous slip and implications for earthquake hazard, *Bull. Seism. Soc. Am.* **81**, 1603–1621.
- Cerjan, C., D. Kosloff, R. Kosloff, and M. Reshef (1985). A nonreflecting boundary condition for discrete acoustic and elastic wave equations, *Geophysics* **50**, 705–708.
- Clayton, R. and B. Engquist (1977). Absorbing boundary conditions for acoustic and elastic wave equations, *Bull. Seism. Soc. Am.* **71**, 1529–1540.
- Cotton, F., M. Campillo, and R. Archuleta (1995). Slip history of the 1994 Northridge earthquake: results and limits of strong motion inversion, *EOS Supplement* **76**, Am. Geophys. Union, 424.
- Davis, T. L., J. Namson, and R. F. Yerkes (1989). A cross section of the Los Angeles Area: Seismically active fold and thrust belt, the 1987 Whittier Narrows earthquake, and earthquake hazard, *J. Geophys. Res.* **94**, 9644–9664.
- Dewey, J. W., L. Dengler, B. G. Reagor, and K. Moley (1995). Spatial variations of intensity in the Northridge earthquake, submitted to *Northridge Earthquake Special Publication*, California Division of Mines and Geology.
- Dolan, J. J., K. Sieh, T. K. Rockwell, R. S. Yeats, J. Shaw, J. Suppe, G. J. Huftile, and E. M. Gath (1995). Prospects for larger or more frequent earthquakes in the Los Angeles Metropolitan region, *Science* **267**, 199–205.
- Faust, L. Y. (1951). Seismic velocity as a function of depth and geologic time, *Geophysics* **16**, 192–206.
- Frankel, A. (1993). Three-dimensional simulations of ground motions in the San Bernardino Valley, California, for hypothetical earthquakes on the San Andreas Fault, *Bull. Seism. Soc. Am.* **83**, 1042–1063.
- Frankel, A. and J. Vidale (1992). A three-dimensional simulation of seismic waves in the Santa Clara Valley, California, from a Loma Prieta aftershock, *Bull. Seism. Soc. Am.* **82**, 2045–2074.
- Fumal, T. E., J. F. Gibbs, and F. R. Edwards (1980). In-situ measurements of seismic velocity at 27 locations in the Los Angeles, California region, *U.S. Geol. Surv. Open-File Rep.* **80-378**.
- Gao, S., H. Liu, P. M. Davis, and D. L. Knopoff (1996). Localized amplification of seismic waves and correlation with damage due to the Northridge earthquake, *Bull. Seism. Soc. Am., Special Issue* **86**, no. 1B, S209–S230.
- Graves, R. (1995). Preliminary analysis of long-period basin response in the Los Angeles region from the 1994 Northridge earthquake, *Geophys. Res. Lett.* **22**, 101–104.
- Hadley, D. and H. Kanamori (1977). Seismic structure of the Transverse Ranges, California, *Geol. Soc. Am. Bull.* **88**, 1469–1478.
- Hartzell, S. H. and T. H. Heaton (1983). Inversion of strong ground motion and teleseismic waveform data for the fault rupture history of the 1979 Imperial Valley, California, earthquake, *Bull. Seism. Soc. Am.* **73**, 1553–1583.
- Hartzell, S. H. and T. H. Heaton (1986). Rupture history of the 1984 Morgan Hill, California, earthquake from the inversion of strong motion records, *Bull. Seism. Soc. Am.* **76**, 649–674.
- Hartzell, S. H. and M. Iida (1990). Source characteristics of the 1987 Whittier Narrows, California, earthquake from the inversion of strong motion records, *J. Geophys. Res.* **95**, 12475–12486.
- Hauksson, E. (1990). Earthquakes, faulting and stress in the Los Angeles basin, *J. Geophys. Res.* **95**, 15365–15394.
- Heaton, T. H., J. F. Hall, D. J. Wald, and M. W. Hallig (1995). Response of high-rise and base-isolated buildings to a hypothetical M_w 7.0 blind thrust earthquake, *Science* **267**, 206–211.
- Hill, J., H. Benz, M. Murphy, and G. T. Schuster (1990). Propagation and resonance of SH waves in the Salt Lake Valley, Utah, *Bull. Seism. Soc. Am.* **80**, 23–42.
- Levander, A. R. (1988). Fourth-order finite-difference P-SV seismograms, *Geophysics* **53**, 1425–1436.
- Ludwig, W. J., J. E. Nafe, and C. L. Drake (1970). Seismic refraction, in *The Sea*, Vol. 4, Part 1, A. E. Maxwell (Editor), Wiley-Interscience, New York, 53–84.
- Madariaga, R. (1976). Dynamics of an expanding circular fault, *Bull. Seism. Soc. Am.* **66**, 163–182.
- Magistrale, H., K. McLaughlin, and S. Day (1996). A geology based 3-D velocity model of the Los Angeles basin sediments, *Bull. Seism. Soc. Am.* **86**, in press.
- Nafe, J. E. and C. L. Drake (1960). Physical properties of marine sediments, in *The Sea* 3, M. N. Hill (Editor), Interscience, New York, 794–815.
- Office of Emergency Services (1994). Building and Safety Damage, Northridge earthquake disaster, DR-1008.
- Olsen, K. B. (1994). Simulation of three-dimensional wave propagation in the Salt Lake Basin, *Ph.D. Thesis*, University of Utah, Salt Lake City, Utah, 157 pp.
- Olsen, K. B. and G. T. Schuster (1992). Seismic hazard analysis in Salt Lake Valley by finite difference simulation of three-dimensional elastic wave propagation, *Scientific Excellence in High Performance Computing: The 1990 IBM Price Papers*, Vol. 1, Sec. 6, Baldwin Press, Athens, Georgia, 135–165.
- Olsen, K. B. and G. T. Schuster (1994). Three-dimensional modeling of the site amplification in East Great Salt Lake Basin, *U.S. Geol. Surv. Tech. Rep.* **1434-93-G-2345**, 102 pp.
- Olsen, K. B., J. C. Pechmann, and G. T. Schuster (1995a). Simulation of 3D elastic wave propagation in the Salt Lake Basin, *Bull. Seism. Soc. Am.* **85**, 1688–1710.
- Olsen, K. B., R. J. Archuleta, and J. R. Matarese (1995b). Three-dimensional simulation of a magnitude 7.75 earthquake on the San Andreas fault, *Science* **270**, 1628–1632.
- Olsen, K. B., J. C. Pechmann, and G. T. Schuster (1996). An analysis of simulated and observed blast records in the Salt Lake Basin, *Bull. Seism. Soc. Am.* **86**, in press.
- Olson, A. H. and R. J. Apsel (1982). Finite faults and inverse theory with applications to the 1979 Imperial Valley earthquake, *Bull. Seism. Soc. Am.* **82**, 1969–2002.
- Pitarka, A. S., H. Takenaka, and D. Suetsugu (1994). Modeling strong motion in the Ashigara valley for the 1990 Odawara, Japan, earthquake, *Bull. Seism. Soc. Am.* **84**, 1327–1335.
- Sánchez-Sesma, F. J. and F. Luzón (1995). Seismic response of three-dimensional valleys for incident P, S, and Rayleigh waves, *Bull. Seism. Soc. Am.* **85**, 269–284.
- Schrievner, C. W. and D. V. Helmberger (1994). Seismic waveform modeling in the Los Angeles Basin, *Bull. Seism. Soc. Am.* **84**, 1310–1326.
- Steidl, J. H., R. J. Archuleta, and S. H. Hartzell (1991). Rupture history of the 1989 Loma Prieta, California, earthquake, *Bull. Seism. Soc. Am.* **81**, 1573–1602.
- Stephenson, W. J., T. K. Rockwell, J. K. Odum, K. M. Shedlock, and D. A. Okaja (1995). Seismic reflection and geomorphic characterization of the onshore Palos Verdes Fault zone, Los Angeles, California, *Bull. Seism. Soc. Am.* **85**, 943–950.
- Takeo, M. and H. Kanamori (1995). Simulation of long-period ground mo-

- tions for the 1923 Kanto earthquake ($M \approx 8$), *Bull. Earthquake Res. Inst. Univ. Tokyo* **67**, 389–486.
- Vidale, J. E. and D. V. Helmberger (1988). Elastic finite-difference modeling of the 1971 San Fernando, California, earthquake, *Bull. Seism. Soc. Am.* **78**, 122–141.
- Virieux, J. (1984). SH-wave propagation in heterogeneous media: velocity-stress finite-difference method, *Geophysics* **49**, 1933–1957.
- Virieux, J. (1986). P-SV wave propagation in heterogeneous media: velocity-stress finite-difference method, *Geophysics* **51**, 889–901.
- Wald, D., D. V. Helmberger, and T. H. Heaton (1991). Rupture model of the 1989 Loma Prieta earthquake from the inversion of strong motion and broadband teleseismic data, *Bull. Seism. Soc. Am.* **81**, 1540–1572.
- Wald, D. J., T. H. Heaton, and K. W. Hudnut (1996). The slip history of the 1994 Northridge, California, earthquake determined from strong-motion, teleseismic, GPS, and leveling data, *Bull. Seism. Soc. Am., Special Issue* **86**, no. 1B, S49–S70.
- Working Group on California Earthquake Probabilities (1995). Seismic hazards in southern California: probable earthquakes, 1994 to 2024, *Bull. Seism. Soc. Am.* **85**, 379–439.
- Wright, T. L. (1991). Structural geology and tectonic evolution of the Los Angeles basin, California, in *Active Margin Basins, AAPG Memoir* **52**, K. T. Biddle (Editor), 35–134.
- Yerkes, R. F., T. H. McCulloh, J. E. Schoellhamer, and J. G. Vedder (1965). *Geology of the Los Angeles Basin California—An Introduction*, U.S. Geol. Surv. Profess. Paper 420-A, Washington, D.C.
- Yomogida, K. and J. T. Etgen (1993). 3-D wave propagation in the Los Angeles basin for the Whittier-Narrows earthquake, *Bull. Seism. Soc. Am.* **83**, 1325–1344.
- Ziony, J. I. (1985). Evaluating earthquake hazards in the Los Angeles region—an earth-science perspective, *U.S. Geol. Surv. Profess. Paper*, 1360.

Institute for Crustal Studies
University of California at Santa Barbara
Santa Barbara, California 93106-1100
(K.B.O., R.J.A.)

Department of Geological Sciences
University of California at Santa Barbara
Santa Barbara, California 93106-1100
(R.J.A.)

Manuscript received 8 September 1995.